Available online at www.sciencedirect.com

SciVerse ScienceDirect

Ceramics International 39 (2013) 7247–7253

CERAMICS INTERNATIONAL

www.elsevier.com/locate/ceramint

Short communication

Preparation of silica encapsulated carbon black with high thermal stability

Cheng Peng, Chuxin Zhang, Ming Lv, Jianqing Wu*

School of Materials Science and Engineering, South China University of Technology, Guangzhou 510640, China

Received 23 November 2012; received in revised form 24 January 2013; accepted 24 January 2013
Available online 1 February 2013

Abstract

A silica encapsulated carbon black has been prepared by a modified emulsion polymerization. After firing above 1000 °C, the product shows high oxidation resistance up to 1200 °C and good stability in frit glaze at 950 °C. The intrinsic mechanism for the high thermal stability is investigated by various techniques. SEM and TEM results show that carbon black nanoparticles are encapsulated by compact amorphous silica and an embedded structure is formed. XPS and FTIR analyses indicate that C–Si–O chemical bonds are present between carbon black and amorphous silica. The embedded structure with strong bonding can separate the carbon black from the outside, reduce the negative effects of mismatch in thermal expansion and thus improve the thermal stability of carbon black.
© 2013 Elsevier Ltd and Techna Group S.r.l. All rights reserved.

Keywords: Carbon black; Silica encapsulation; Thermal stability; Emulsion polymerization; Ceramic pigment

1. Introduction

Recently, assembly of two materials at micro/nanoscale has attracted considerable interest for its use in the design and fabrication of advanced materials [1,2]. The properties of the as-generated materials, such as core–shell structures, cables and capsules, can be optionally tuned or integrated by tailoring the size and parameter of the components [3–6]. In ceramic industry, encapsulation of colorants by a stable matrix, zircon or silica, is a usual solution to produce high temperature pigments, since these matrixes can effectively protect the colorants against chemical reactions, e.g. SiO_2–Fe_2O_3 pigment [7], $ZrSiO_4$–$CdS_{1-x}Se_x$ pigment [8].

The ceramic pigments with deep black hue are always cobalt-containing and thus expensive. Meanwhile, the introduction of cobalt also causes environmental problems [9]. Therefore, there are economic and ecological advantages to find alternative materials. Carbon black (CB) is commonly used as black pigment at room temperature ascribing to its high tinting strength and low cost. Unfortunately, the application of CB in ceramic seems to be impossible due to its oxidation above 600 °C. In literature, the dominant methods for oxidation protection of carbon materials involve the use of a coating [10,11] or surface treatment [12]. However, these methods have met with limited success at high temperature due to coating irregularities and mismatch in thermal expansion. Wang et al. reported the preparation of silica coated carbon black by a combustion method [13] but further efforts are needed to understand the stabilizing mechanism and to improve their thermal stability for industrial use.

This work reports a modified emulsion polymerization method for the preparation of silica encapsulated carbon black (SECB). The thermal stability of the SECB obtained at varied temperatures was evaluated and the stabilization mechanism was proposed based on morphological observations and chemical bonding analyses.

2. Materials and methods

2.1. Chemicals

Carbon black (JE-2105) with surface area of 179.2 m^2/g was purchased from China Synthetic Rubber Corporation and dispersed by polyvinylpyrrolidone (PVP-30). Tetraethyl orthosilicate (TEOS, 98%) was used as the silica source.

*Corresponding author. Tel.: +86 20 8711 1669; fax: +86 20 8711 0273.
E-mail addresses: ceramicgroup@163.com, imjqwu@scut.edu.cn (J. Wu).

0272-8842/$ - see front matter © 2013 Elsevier Ltd and Techna Group S.r.l. All rights reserved.
http://dx.doi.org/10.1016/j.ceramint.2013.01.078

Hexadecyl trimethyl ammonium bromide (CTAB) was selected as the surfactant and n-butanol as co-surfactant. Ammonium hydroxide ($NH_3 \cdot H_2O$, 25–28 wt%) was adopted to adjust the pH value. Distilled water was used in all preparations.

2.2. Sample preparation

0.2 g CB was put into a beaker with 10 ml PVP solution (6×10^{-4} M). After stirring for 24 h, 1 ml $NH_3 \cdot H_2O$ was introduced, and then the suspension was added dropwise to another beaker including 20 g TEOS, 5 g n-butanol, and 5 g CTAB under vigorous stirring. Subsequently, the mixture was ultrasonically treated for 5 min to form a gel. The gel was aged for 24 h, dried at 105 °C for 6 h and heated at varied temperatures in air. During the heat treatment, the furnace was held at different temperatures, 900 °C, 950 °C, 1000 °C, 1050 °C, 1100 °C, 1150 °C and 1200 °C. A platinum crucible with the dry gel was put into the furnace chamber, soaked for 30 min, and taken out for natural cooling. The samples obtained at these temperatures were labeled H900, H950, and the like. The dry gel was denoted as H0.

20 g homemade transparent frit (chemical formula: SiO_2 45.5%, $BaCO_3$ 4.0%, $Al(OH)_3$ 17.0%, KNO_3 9.5%, Na_2CO_3 19.0%, $MgCO_3$ 1.5%, Na_2SiF_6 2.4% and $CaCO_3$ 1.1%) and about 10 ml distilled water were mixed in a ball miller to form glaze slurry. 0.1 g H1000 powder was added into 1 g slurry and then the slurry was laid on porcelain tiles. The tiles were fired to desired temperature at a rate of 40 °C/min and soaked for 5 min.

2.3. Characterization

The crystalline phases of raw CB, sample H0 and H1200 were identified by X-ray diffractometer (PANalytical X'pert PRO, Almelo, Netherlands), using CuKα radiation, with a step size of 0.033° and scan step time of 5.08 steps/s. Thermogravimetry (TG) and differential scanning calorimetry (DSC) were performed using a Netzsch Model 449C instrument for raw CB, H0 and H1200. Approximately 7 mg sample was heated with 10 °C/min in air flow, using Al_2O_3 as the reference material. The thermal stability of CB in all samples was evaluated by the L^* (luminance) value according to CIE 1976 ($L^*a^*b^*$) coordinates, which was measured by a colorimeter (X-rite 8200, Grand Rapids, Michigan), with the D_{65} illuminant, 10^o angle vision and $ZrSiO_4$ glaze as white reference. The microstructure of CB, H0, H900, H1000 and H1200 was observed using a scanning electronic microscope (SEM, ZEISS EVO 18, Oberkochen, Germany) with operating voltage 10 kV and working distance 10 mm, and transmittance electronic microscope (TEM; JEM 2010, JEOL, Tokyo, Japan) with operating voltage 200 kV. The chemical compositions and chemical bonds of H1000 were identified by an X-ray photoelectron spectroscopy (XPS; Axis Ultra DLD, Kratos, UK). Prior to XPS analysis, the composite powder was ground to break the encapsulation structure. The C 1s (284.5 eV) peak was used for the calibration of the spectrum and binding energy values were corrected for the charging effect. Furthermore, the reactions between the components were studied by fourier transform infrared spectroscopy (FTIR; Vector33, Bruker, Germany) using KBr pressed disk technique. Raw CB, sample H0 and H1000 were selected for comparation. Before FTIR analysis, H0 was calcined at 550 °C for 2 h to remove the residual CTAB.

3. Results and discussion

3.1. Phase composition and thermal analysis

Fig. 1 shows the XRD patterns of raw CB, sample H0 and sample H1200. In Fig. 1a, the XRD pattern can be readily indexed to carbon (PDF 26-1076). In Fig. 1b, the crystal phase of H0 can be matched to residual CTAB (PDF 25-1588). A broad background peak comes from the hydration product of TEOS, possibly a mixture of $Si(OH)_4$, Si–O–Si and SiO_2, depending on the extent of hydration [14,15]. In Fig. 1c, the XRD pattern of H1200 shows a broad peak of amorphous structure, revealing that the crystallization process which will probably result in apparent morphological changes has not occurred at 1200 °C.

The TG–DSC curves of raw CB, sample H0 and H1200 are shown in Fig. 2. Fig. 2a reveals that CB begins to oxidize at 650 °C, and burns out at about 800 °C. In Fig. 2b, the TG curve of H0 exhibits several mass loss features. The endothermal peaks with slight mass loss at 80 °C can be explained as the removal of the reabsorbed water. The two exothermic peaks centered at 550 °C and 740 °C are attributed to the oxidation of residual organics and CB, respectively. The endothermal peaks at 480, 690 and 780 °C are probably due to the decomposition of TEOS hydration product. In Fig. 2c, the TG curve shows a

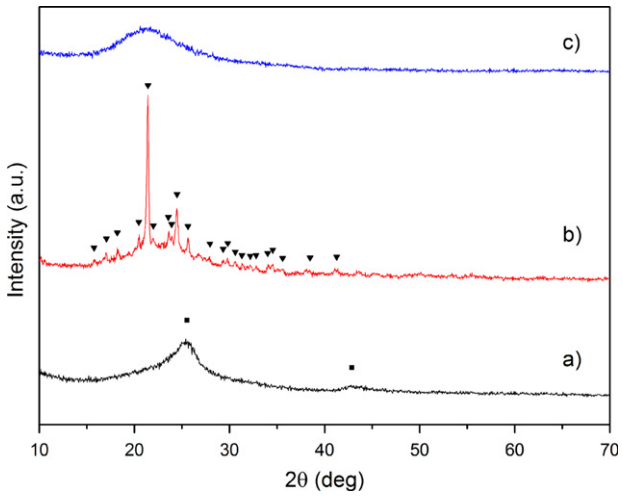

Fig. 1. XRD patterns of (a) raw carbon black, (b) H0 and (c) H1200.

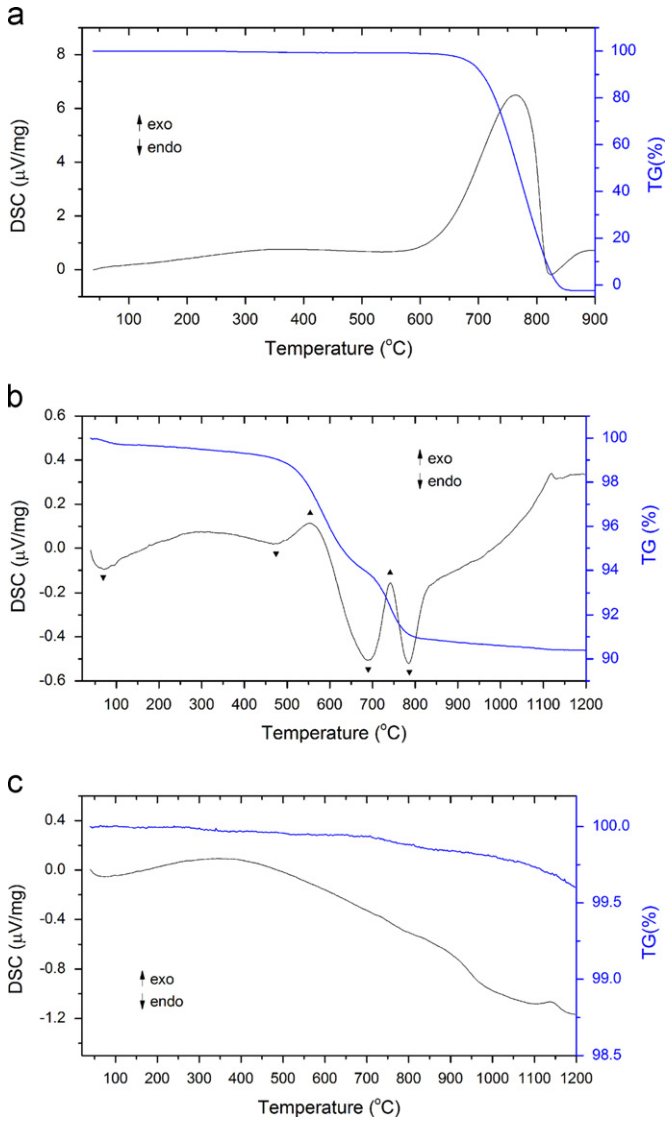

Fig. 2. TG–DSC curves of (a) raw carbon black, (b) H0 and (c) H1200.

weak mass loss from room temperature to 1200 °C, indicating a slow oxidation process of CB in the sample H1200.

3.2. Thermal stability

According to CIE (1976) standard, L^* value ranges from 0 to 100, corresponding to dark black and bright white. L^* value of pure CB at room temperature is 14.68. L^* value of the composite powder basically depends on the remaining amount of CB. As a result, the thermal stability of the samples can be evaluated by measuring L^* value after calcination. Fig. 3a shows L^* values of the samples obtained at different temperatures. As the temperature increases, L^* values of the samples rapidly decreases at first, but slowly increases after 1000 °C. In these samples, L^* values are dominated by the co-effect of the rate of CB oxidation and formation of SiO_2 encapsulation. At 900 °C, L^* value is up to 98.04 since CB is exposed to air and

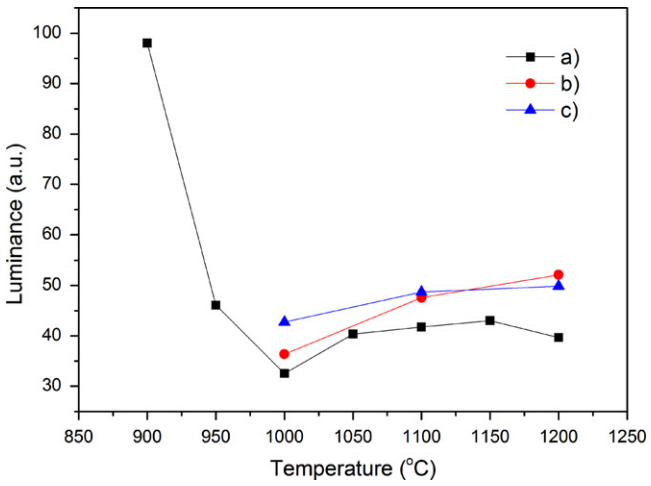

Fig. 3. (a) Luminance values of the samples obtained at different temperatures; luminance values of (b) H1000 and (c) H1200 calcined at different temperatures for 30 min in air.

quickly burns out. At 1000 °C, L^* value is drastically reduced to 32.54. We suppose that compact encapsulation is formed and the oxidation is effectively prohibited at this temperature. The slight decrease at 1200 °C is probably attributed to the positive effect of quick formation of SiO_2 encapsulation. Fig. 3b and c shows L^* values of sample H1000 and H1200 calcined at different temperatures. Both of the L^* values gradually increase with increase in temperature, indicating slow oxidation of CB in the composites, which is consistent with thermal analysis.

It is known to us that the alkali and alkaline-earth components in glaze can destroy SiO_2 encapsulation and depress the thermal stability of CB. We evaluated the thermal stability of SECB in homemade frit glaze and the result is shown in Fig. 4. In Fig. 4a, the glaze surface is dark black with a surface L^* value of 36.25, close to the L^* value of sample H1000, indicating that the protection of CB is almost not affected by glaze at 950 °C. While sintered at 1000 °C, the surface is gray in color with a surface L^* value of 53.73, which is considerably higher than that of sample H1000, demonstrating the corrosion effect of glaze on SiO_2 encapsulation. Although the SECB powders can withstand high temperature calcination, the thermal and chemical stability still needs to be improved for industrial application.

3.3. Morphological observation

The morphology of the obtained samples was observed by SEM (Fig. 5). It can be seen in Fig. 5a that the CB particles are about 50 nm in size and well dispersed by PVP. In Fig. 5b, sample H0 is composed of many spheres which aggregate to clusters. The spheres are about 500 nm in diameter, much larger than CB particles. When calcined at 900 °C, the decomposition of TEOS hydration product into amorphous SiO_2 makes the particles porous and apparently coarse in SEM image (Fig. 5c). At 1000 °C,

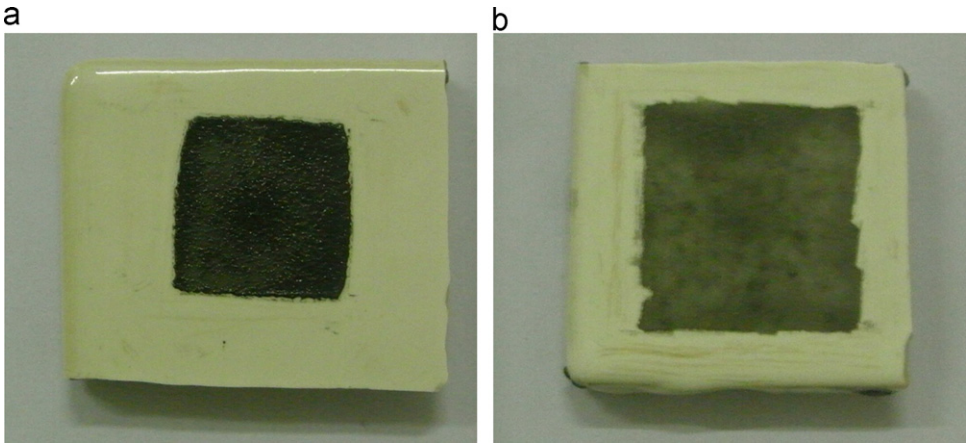

Fig. 4. Photographs of the SECB frit glaze sintered at (a) 950 °C and (b) 1000 °C.

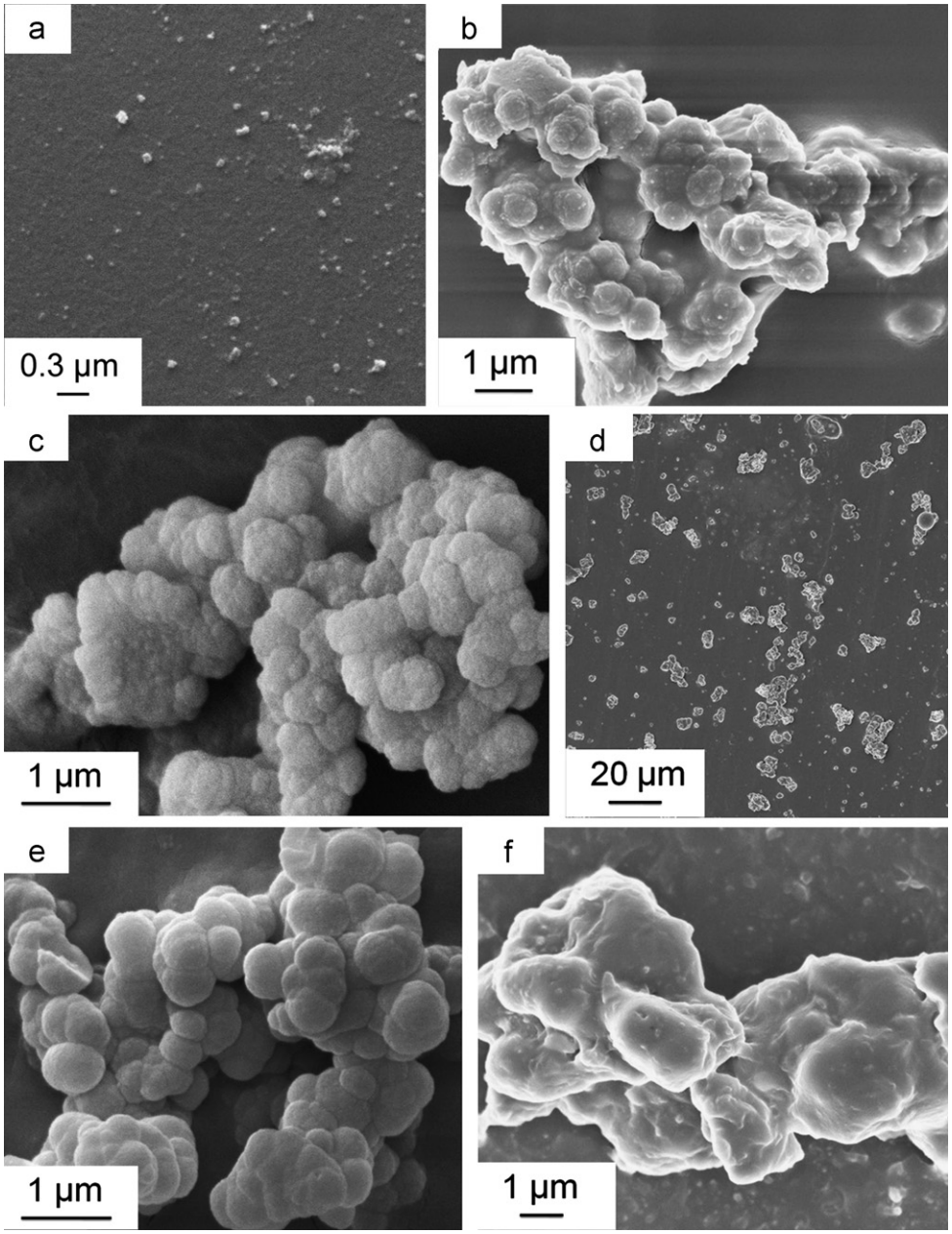

Fig. 5. SEM images of (a) PVP dispersed CB, (b) H0, (c) H900, (d), (e) H1000 and (f) H1200.

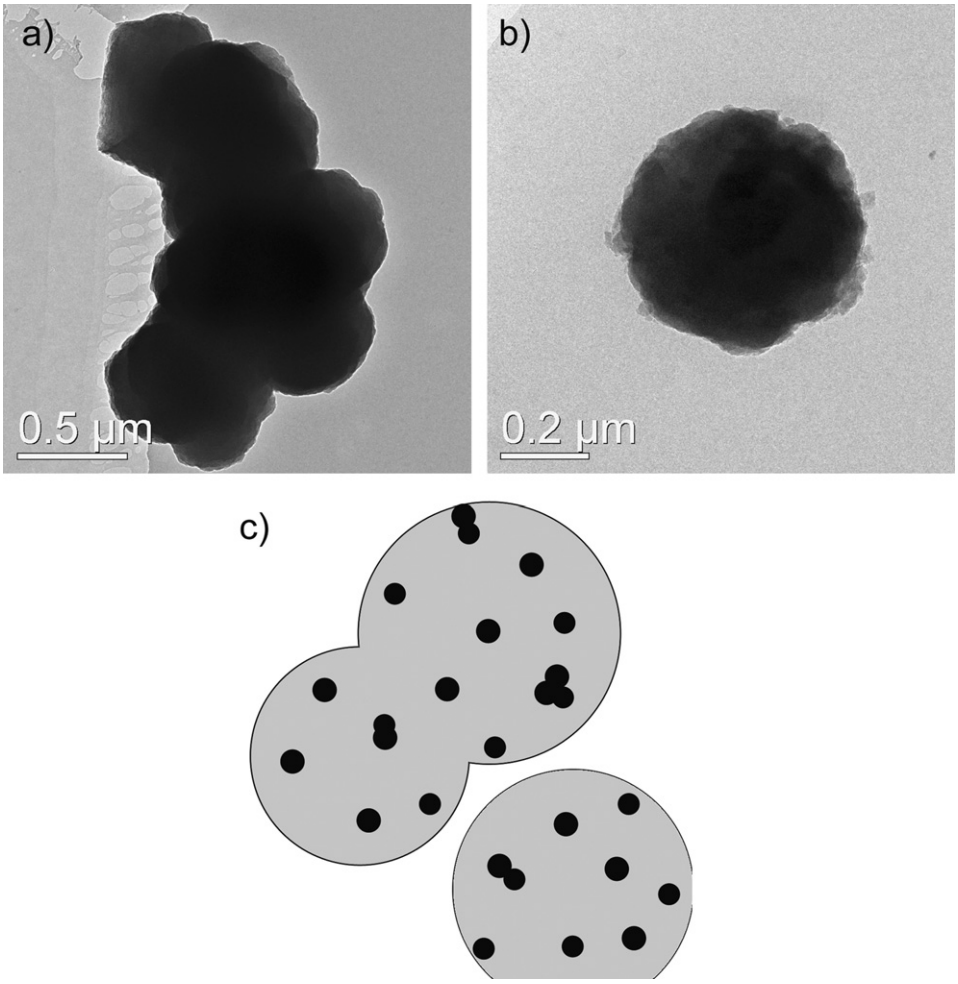

Fig. 6. (a) and (b) TEM images of H1000 and (c) schematic diagram of the structure.

the particles become smooth, indicating the formation of compact encapsulation by vitrification (Fig.5 d and e). This gives a direct evidence of why sample H1000 shows the lowest L^* value. At 1200 °C, the particles look smoother and fuse together to a considerable extent (Fig. 5f), due to the surface diffusion driven by the pressure difference at high temperature [16]. Although the spheres severely aggregate at this temperature, CB particles are still effectively encapsulated by SiO_2.

The morphology of H1000 was also observed by TEM (Fig. 6a). The particles show dark contrast because they are too thick to be penetrated by an electron beam. In the enlarged image (Fig. 6b), a contrast difference between the rim and the center like core–shell structures is not observed. According to SEM results, the SiO_2 spheres are much larger than CB particles. We think that SiO_2 spheres encapsulate many CB nanoparticles simultaneously, as illustrated by schematic diagram of the structure in Fig. 6c. Such an embedded structure is useful to eliminate the thermal expansion mismatch in thermal cycles since the thermal stress can be homogeneously scattered. Based on these morphological observations, we can conclude that the compact SiO_2 encapsulation on CB nanoparticles with embedded structure is formed by vitrification above 1000 °C.

3.4. The mechanism for the high thermal stability

To study the intrinsic mechanism for the thermal stability, XPS analysis was carried out to examine the chemical bonding of H1000. The XPS survey spectrum (Fig. 7a) indicates the peaks of all the elements from CB and SiO_2, i.e. Si, C and O. Fig. 7b and c shows XPS narrow scans of Si 2p and C 1s. Based on previous studies [17,18], the Si 2p spectrum can be decomposed into two peaks corresponding to O–Si–C (101.6 eV) and Si–O (102.7 eV), while the spectrum of C 1s is fitted with two peaks corresponding to C–Si–O (283.5 eV) and C–C (284.6 eV). This result demonstrates that C–Si–O chemical bonds are present between CB and SiO_2 encapsulation.

The samples were further analyzed by FTIR. For comparison, raw CB, H0 and H1000 were selected and the results are shown in Fig. 8. The bands at 3440 cm^{-1} and 1640 cm^{-1} arise from the O–H bond stretching modes of absorbed water. The bands at 1100 cm^{-1} and 470 cm^{-1} belong to asymmetrical stretch vibration and bending

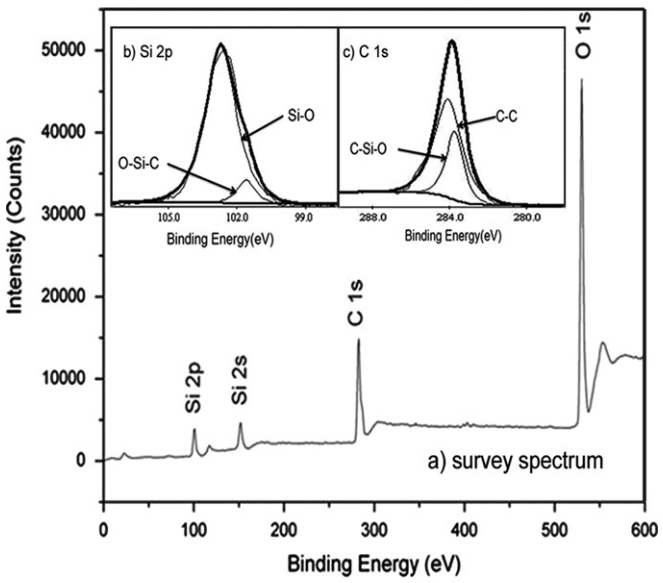

Fig. 7. (a) XPS survey spectrum of H1000; XPS narrow-scan spectra of (b) Si 2p and (c) C 1s.

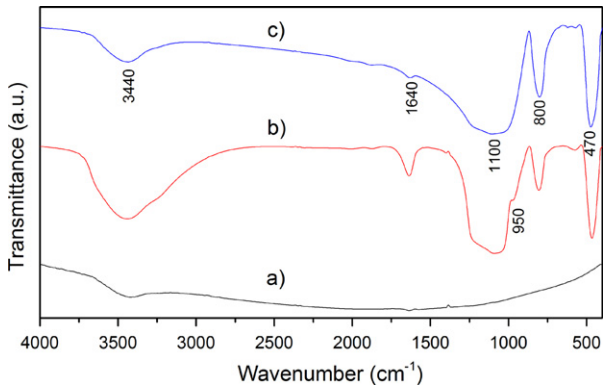

Fig. 8. FTIR spectra of (a) raw carbon black, (b) H0 calcined at 550 °C and (c) H1000.

vibration of Si–O–Si. The band at 950 cm^{-1} which disappears after heating at 1000 °C results from the stretch vibration of Si–OH. It should be noted that the band at 800 cm^{-1} is detected. This band is due to the incorporation of oxygen atoms in Si–C bonds which shifts from 780 cm^{-1} [17,19]. FTIR result further confirms the presence of C–Si–O chemical bonds between CB and SiO_2 encapsulation. The embedded structure with strong bonding can separate the carbon black from the outside, reduce the negative effects of mismatch in thermal expansion and improve the thermal stability of CB.

4. Conclusions

In summary, silica encapsulated carbon black has been prepared by a modified emulsion polymerization method. After firing above 1000 °C, the product shows high oxidation resistance up to 1200 °C and good stability in glaze at 950 °C. The embedded structure and the strong chemical bonding between the SiO_2 encapsulation and CB are thought to be responsible for their excellent thermal stability. The results of this work demonstrate the possibility of SECB as high temperature pigment but the thermal stability needs to be further improved for industrial application. In addition to the encapsulation of CB, this method might be useful for the fabrication of advanced materials which need to go through a high temperature process.

Acknowledgment

This work was financially supported by the Foundation for Distinguished Young Talents in Higher Education of Guangdong, China (LYM10017).

References

[1] P.V. Kamat, Meeting the clean energy demand: nanostructure architectures for solar energy conversion, Journal of Physical Chemistry C 111 (2007) 2834–2860.
[2] C.B. Murray, C.R. Kagan, M.G. Bawendi, Synthesis and characterization of monodisperse nanocrystals and close-packed nanocrystal assemblies, Annual Review of Materials Science 30 (2000) 545–610.
[3] I.G. Loscertales, A. Barrero, I. Guerrero, R. Cortijo, M. Marquez, A.M. Ganan-Calvo, Micro/nano encapsutation via electrified coaxial liquid jets, Science 295 (2002) 1695–1698.
[4] S.M. Marinakos, J.P. Novak, L.C. Brousseau, A.B. House, E.M. Edeki, J.C. Feldhaus, D.L. Feldheim, Gold particles as templates for the synthesis of hollow polymer capsules. Control of capsule dimensions and guest encapsulation, Journal of the American Chemical Society 121 (1999) 8518–8522.
[5] F. Fabbri, F. Rossi, G. Attolini, G. Salviati, B. Dierre, T. Sekiguchi, N. Fukata, Luminescence properties of SiC/SiO_2 core–shell nanowires with different radial structure, Materials Letters 71 (2012) 137–140.
[6] C. Huber, C. Elissalde, V. Hornebecq, S. Mornet, M. Treguer-Delapierre, F. Weill, M. Maglione, Nano-ferroelectric based core–shell particles: towards tuning of dielectric properties, Ceramics International 30 (2004) 1241–1245.
[7] M. Llusar, V. Royo, J.A. Badenes, M.A. Tena, G. Monrós, Nanocomposite Fe_2O_3–SiO_2 inclusion pigments from post-functionalized mesoporous silicas, Journal of the European Ceramic Society 29 (2009) 3319–3332.
[8] B.E. Yekta, M. Tamizifar, N. Rahimi, Synthesis of a zircon–cadmium sulfo selenide pigment by a sol–gel technique, Journal of Ceramic Society of Japan 115 (2007) 757–760.
[9] S.H. He, Z.W. Lin, A.F. Yang, X.J. Wang, C. Chen, H.L. Yang, Investigation on heavy metal pollution of Co and Cu mine waste dump in Changjiang Hainan Province of China, The Administration and Technique of Environmental Monitoring 24 (2012) 41–46.
[10] W.P. Hoffman, H.T. Phan, A. Groszek, The deposition of silica on carbon as a model system for oxidation protection coatings, Carbon 33 (1995) 509–524.
[11] C.C. Landry, A.R. Barron, MOCVD of alumina–silica oxidation resistant coatings on carbon fibers, Carbon 33 (1995) 381–387.
[12] T. Durkic, A. Peric, M. Lausevic, A. Dekanski, O. Neskovic, M. Veljkovic, Z. Lausevic, Boron and phosphorus doped glassy carbon: I. Surface properties, Carbon 35 (1997) 1567–1572.
[13] X. Wang, Q. Chang, Q. Bao, X. Zhang, Preparation and characterization of coated carbon black pigment, Key Engineering Materials 512-515 (2012) 284–287.
[14] S.L. Chen, P. Dong, G.H. Yang, J.J. Yang, Kinetics of formation of monodisperse colloidal silica particles through the hydrolysis and

condensation of tetraethylorthosilicate, Industrial and Engineering Chemistry Research 35 (1996) 4487–4493.
[15] C. Peng, M. Lv, The breaking effect of F^- ions on bridging Si–O bonds under alkaline hydrothermal conditions, Materials Letters 92 (2013) 393–396.
[16] W.D. Kingery, H.K. Bowen, D.R. Uhlmann, Introduction to Ceramics, 2nd ed., Wiley, New York, 1976.
[17] Y.H. Wang, M.R. Moitreyee, R. Kumar, L. Shen, K.Y. Zeng, J.W. Chai, J.S. Pan, A comparative study of low dielectric constant barrier layer, etch stop and hardmask films of hydrogenated amorphous Si–(C, O, N), Thin Solid Films 460 (2004) 211–216.
[18] G.R. Lin, T.C. Lo, L.H. Tsai, Y.H. Pai, C.H. Cheng, C.I. Wu, P.S. Wang, Finite silicon atom diffusion induced size limitation on self-assembled silicon quantum dots in silicon-rich silicon carbide, Journal of the Electrochemical Society 159 (2011) K35–K41.
[19] Y. Chen, C. Wang, B. Zhu, Y. Wang, Y. Liu, T. Tan, R. Gao, X. Lin, F. Meng, Growth of SiC whiskers from hydrogen silicone oil, Journal of Crystal Growth 357 (2012) 42–47.